Structure−Activity Relationships for the Interaction of Bovine Pancreatic Trypsin Inhibitor with an Intracellular Site on a Large Conductance Ca^{2+}-Activated K^+ Channel†

Isabelle Favre,‡ Guy W. J. Moss,‡,§ David P. Goldenberg,|| Jacek Otlewski,⊥ and Edward Moczydlowski*,‡,#

Departments of Pharmacology and of Cellular and Molecular Physiology, Yale University School of Medicine, Sterling Hall of Medicine, P.O. Box 208066, New Haven, Connecticut 06520-8066, Department of Biology, University of Utah, Salt lake City, Utah 84112, and Institute of Biochemistry and Molecular Biology, University of Wroclaw, 50-137 Wroclaw, Poland

Received September 14, 1999

ABSTRACT: Large conductance Ca^{2+}-activated K^+ channels (BK_{Ca}) contain an intracellular binding site for bovine pancreatic trypsin inhibitor (BPTI), a well-known inhibitor of various serine proteinase (SerP) enzymes. To investigate the structural basis of this interaction, we examined the activity of 11 BPTI mutants using single BK_{Ca} channels from rat skeletal muscle incorporated into planar lipid bilayers. All of the mutants induced discrete substate events at the single-channel level. The dwell time of the substate, which is inversely related to the dissociation rate constant of BPTI, exhibited relatively small changes (<9-fold) for the various mutants. However, the apparent association rate constant varied up to 190-fold and exhibited a positive correlation with the net charge of the molecule, suggesting the presence of a negative electrostatic surface potential in the vicinity of the binding site. The substate current level was unaffected by most of the mutations except for substitutions of Lys15. Different residues at this position were found to modulate the apparent conductance of the BPTI-induced substate to 0% (K15G), 10% (K15F), 30% (K15 wild-type), and 55% (K15V) of the open state at +20 mV. Lys15 is located on a loop of BPTI that forms the primary contact region for binding to many SerPs such as trypsin, chymotrypsin, and elastase. The finding that Lys15 is a determinant of the conductance behavior of the BK_{Ca} channel when BPTI is bound implies that the same inhibitory loop that contacts SerP's is located close to the protein interface in the BK_{Ca} channel complex. This supports the hypothesis that the C-terminal region of the BK_{Ca} channel protein contains a domain homologous to SerP's. We propose a domain interaction model for the mechanism of substate production by Kunitz inhibitors based on current ideas for allosteric activation of BK_{Ca} channels by voltage and Ca^{2+}.

Large conductance Ca^{2+}-activated K^+ channels (BK_{Ca})[1] are members of the P-region superfamily of proteins that function as ion channels selective for Na^+, Ca^{2+}, or K^+ (*1*). Major physiological functions of BK_{Ca}s include regulation of transmitter release by facilitating repolarization at presynaptic nerve terminals and hyperpolarization of smooth muscle cells as a negative feedback mechanism to control contractile tone (*2*). The ∼125 kDa channel-forming α-subunit of BK_{Ca} is among the largest known integral membrane proteins that form highly K^+-selective channels as a homotetramer. A region of ∼210 residues near the N-terminus of BK_{Ca} is homologous to the S1−S6 motif of voltage-sensitive K_V channels (*3*, *4*). S1−S6 corresponds to six membrane-spanning segments and also contains a highly conserved P-region segment between S5 and S6. The C-terminal portion of the P-region forms the ion-selectivity filter of K^+ channels as identified in the crystal structure of KcsA, a small bacterial K^+ channel protein (*5*). The S1−S6 region of BK_{Ca} also contains a recognizable S4 motif known to be associated with voltage-sensitive activation. Much less is known about the function of the ∼800 residue C-terminal portion of BK_{Ca}. This region appears to consist of a cytosolic domain that contains binding sites for intracellular Ca^{2+} involved in channel activation (*6*, *7*) and recognition sites for interacting proteins and regulatory proteins such as protein kinases (*8*−*10*).

One approach to investigating the domain structure of channel proteins involves the use of small protein inhibitors that bind to specific sites and modify functions such as ion permeation and gating of the pore. For example, the charybdotoxin family of scorpion toxins has been successfully used to map residues of the outer vestibule of the

† I.F. and G.W.J.M. contributed equally. This work was supported by grants to E.M. from NIH (GM-51172) and AHA (95008820). I.F. received fellowship support from the AHA (CT Affiliate) and the Swiss National Science Foundation.

* To whom correspondence should be addressed. Phone: (203) 785-4552. Fax: (203) 785-7670. E-mail: edward.moczydlowski@yale.edu.

‡ Department of Pharmacology, Yale University School of Medicine.

§ Present address: Department of Pharmacology, University College of London, London WC1E 6BT, England.

|| University of Utah.

⊥ University of Wroclaw.

Department of Cellular and Molecular Physiology, Yale University School of Medicine.

[1] Abbreviations: APP, amyloid β-protein precursor; BK_{Ca}, large conductance Ca^{2+}-activated K^+ channel; BPTI, bovine pancreatic trypsin inhibitor; KID, Kunitz inhibitor domain of amyloid β-protein precursor; Mops, 3-(*N*-morpholino)propanesufonic acid); SerP, serine proteinase.

10.1021/bi992140v CCC: $19.00
Published on Web 02/02/2000

Drosophila Shaker K_V channel (*11*−*13*). Residues mapped by this technique have been found to lie in an expected arrangement on the extracellular surface of the homologous KcsA protein (*14*). In principle, a similar approach could provide structural information on the intracellular architecture of BK_{Ca}. Our laboratory has previously identified Kunitz inhibitor proteins such as BPTI and dendrotoxin I (DTX-I) as a class of molecules that modify the function of BK_{Ca} in a specific fashion from the intracellular side (*15*, *16*). At the single-channel level, this interaction can be assayed by the production of discrete substate events that correspond to individual residence times of BPTI or DTX-I on a site located outside the intracellular entrance to the pore. Several lines of evidence have led to the hypothesis that the binding site for these inhibitors corresponds to a C-terminal region of BK_{Ca} that is structurally related to the family of serine proteinase (SerP) enzymes (*17*, *18*). This hypothesis predicts that the primary inhibitory loop of BPTI (residues 11−19) that is known to bind in the active site of trypsin would also serve as the principal contact region between BPTI and BK_{Ca}. Initial support for this idea was obtained in experiments which demonstrated that the stable trypsin−BPTI complex ($K_D = 6 \times 10^{-14}$ M) is inactive toward BK_{Ca} (*18*). This latter experiment suggests that an unobstructed inhibitory loop of BPTI is required for binding to BK_{Ca}; however, it does not prove that residues in this loop actually contact the channel protein.

To pursue this question, we have taken advantage of BPTI mutants generated by laboratories interested in the mechanism of protein folding (*19*) or the interaction of BPTI with SerP enzymes (*20*). We analyzed the interaction of 11 mutants involving nine different residues of BPTI with single BK_{Ca} channels of rat skeletal muscle incorporated into planar lipid bilayers. Seven of the tested mutants retain high affinity and specificity for trypsin since the mutations are located at residues of BPTI other than Lys15, a residue known to bind in the substrate specificity pocket of trypsin. These particular mutants exhibited little change in the BK_{Ca} interaction other than variations in the magnitude of the association rate constant, a kinetic parameter that is controlled by a long-range electrostatic interaction. In contrast, four of the tested BPTI mutants, which have substitutions at Lys15 and are weak inhibitors of trypsin, exhibited dramatic changes in the absolute current level and I−V behavior of BPTI-induced substate events. The appearance of substates results from the unavoidable filtering of a rapidly fluctuating gating process that inhibits ion conduction through the BPTI-occupied channel (*21*). Therefore, the finding described in this paper, that a residue critical for the interaction of BPTI with trypsin also has a major impact on BK_{Ca} function, is suggestive of structural relatedness and supports the hypothesis of a SerP-like domain in the BK_{Ca} channel protein.

EXPERIMENTAL PROCEDURES

BPTI, BPTI Mutants, and KID. BPTI and bovine trypsin were purchased from Sigma Chemical Co. (St. Louis, MO). The concentration of BPTI and trypsin was based on quantitative amino acid analysis performed by the Yale Protein Chemistry Facility. The following seven point mutants of BPTI were produced in the laboratory of Dr. David P. Goldenberg at the University of Utah: G12D, A16T, G28K, Y35D, G36D, E49A, and R53A. These mutations were generated by site-directed mutagenesis of a wild-type gene for BPTI expressed in *Escherichia coli* (*22*, *23*). The mutant BPTIs were purified from extracts of *E. coli* by ion-exchange and gel filtration chromatography (*19*). These particular BPTI mutants are stoichiometric inhibitors of trypsin, and their concentration was determined by trypsin titration (*24*).

Three BPTI mutants with substitutions at Lys15 (K15V, K15G, and K15F) were produced in the laboratory of Dr. Jacek Otlewski at the University of Wroclaw, Poland. These mutants were expressed in *E. coli*, cleaved from a fusion protein by cyanogen bromide, and purified by reversed-phase HPLC as described (*20*). These three Lys15 mutants also contained a conservative substitution of M52L to enable specific chemical cleavage of the fusion protein at methionine. The identity of the purified proteins was confirmed by electrospray mass spectroscopy, which gave molecular masses within 1 atomic mass unit of the expected value. The equilibrium constants of these BPTI variants for inhibition of bovine β-trypsin, salmon anionic trypsin, bovine α-chymotrypsin, and human neutrophil elastase have been reported (*20*). Of these four enzymes, the K15V and K15G mutants have the highest affinity for elastase, with K_Ds of 1.6×10^{-10} and 2.1×10^{-6} M, respectively. The K15F mutant exhibits the highest affinity for chymotrypsin ($K_D = 4 \times 10^{-10}$ M).

A variant of BPTI with two substitutions, K15V, R17L, and a deletion of Pro2, was obtained through the courtesy of Dr. Paul Tamburini of Bayer Corporation (West Haven, CT). This mutant was produced by a yeast expression system and is active as a stoichiometric inhibitor of human neutrophil elastase. Dr. Tamburini's laboratory also produced a 56-residue Kunitz inhibitor domain (KID, Figure 7) of human amyloid β-protein precursor (APP) by solid-phase synthesis *(25)*. This inhibitor domain has a peptide backbone fold that is virtually identical to BPTI except for a Gly−Gly−Asn sequence (corresponding to residues 39−41 of BPTI) that adopts a different conformation (*26*). Active KID protein was purified by affinity chromatography on a trypsin-agarose column followed by reversed-phase HPLC. Its molecular weight was confirmed by fast-atom bombardment mass spectroscopy (*25*). KID inhibits trypsin with an affinity of 10^{-10} M (*27*). The concentration of active KID was also determined by trypsin titration.

Planar Bilayer Recording. Plasma membrane vesicles from rat skeletal muscle were prepared as described (*28*) and used as a source of native BK_{Ca} channels for incorporation into planar lipid bilayers. Planar bilayers were formed by painting a 25 mg/mL lipid solution with a fine glass rod on a hole with a diameter of 200 μm in a polystyrene chamber from Warner Instruments (Hamden, CT). Membrane thinning and bilayer formation was monitored by capacitance measurement. The lipid solution was either a 4:1 mixture of bovine brain phosphatidylethanolamine/1,2-diphytanoylphosphatidylcholine or 1-palmitoyl-2-oleoyl-*sn*-glycero-3-phosphoethanolamine/1-palmitoyl-2-oleoyl-*sn*-glycero-3-phosphocholine (Avanti Polar Lipids, Alabaster, AL) in *n*-decane. The solution on both sides of the bilayer was 50 mM KCl and 10 mM Mops-KOH, pH 7.4. During channel incorporation the $CaCl_2$ concentration was 200 μM on the side of the bilayer to which membrane vesicles were added (cis). EDTA (0.1 mM) was added to the opposite side (trans) to establish the orientation of active BK_{Ca} channels as cis-intracellular.

Only bilayers containing single BK_{Ca} channels were used for the experiments. Ca^{2+} concentration on the cis side was sometimes increased as necessary up to 800 μM to maintain open state probability at $\geq$0.90 for measurement of BPTI dwell times and to collect I−V data in the negative voltage range.

Single-channel currents were recorded at room temperature (20−23 °C) using a commercial patch-clamp amplifier. The patch-clamp headstage was connected to the two bilayer chambers using Ag/AgCl electrodes and agar-KCl bridges. Single-channel records typically lasting 1−3 h/bilayer were stored on VCR tape using a digital data recorder and subsequently filtered at a final corner frequency of 20−500 Hz using an 8-pole low-pass Bessel filter as required for analysis or display. Digital sampling of single-channel data was always performed at greater than five times the filter frequency.

Single-Channel Analysis. PCLAMP (Axon Instruments, Foster City, CA) and TAC (Instrutech Corp., Port Washington, NY) software was used for computer-assisted analysis of single-channel data. Current−voltage behavior of the open state or BPTI-induced substates was analyzed by measuring unitary current levels at holding voltages in the range of −50 to +60 mV. The zero-current level was defined by resolved closed states or discrete Ba^{2+}-blocking events induced by addition of 2 μM Ba^{2+} to the intracellular side of the channel. The mean current level of the open state and BPTI-induced substates was measured from appropriately filtered signals by mouse-driven cursors or from peaks of all-points amplitude histograms. Rectifying I−V curves for BPTI-induced substates (e.g., Figure 4) were fit to a two-state model of a simple voltage-dependent process as described previously (*21*). In this model, the apparent subconductance state induced by BPTI arises from filtering of rapid fluctuations between a brief open state and brief closed state of the channel that occur when BPTI is bound. This fluctuation is governed by a voltage-dependent equilibrium constant, $K(V)$, which is the ratio of probabilities at equilibrium that the channel is in the brief open state relative to the brief closed state. The mean substate current, I_{SUB}, is related to the open channel current, I_{OPEN}, by the following equations:

$$I_{SUB} = I_{OPEN}K(V)/[K(V) + 1] \quad (1)$$

$$K(V) = K_0 \exp(-z'FV/RT) \quad (2)$$

where V is the membrane voltage, K_0 is the value of $K(V)$ at 0 mV, z' is an apparent gating charge, and RT/F equals 25.4 mV at 22 °C. Nonlinear curve fitting to eq 1 was performed using Sigmaplot (SPSS Inc., Chicago, IL) software.

Rate constants for binding of BPTI and mutants were measured from histograms of substate dwell times and inter-substate durations, as described previously (*29*). Histograms of such events were well-described by single-exponential distributions. The first-order rate constant for BPTI dissociation was calculated as the reciprocal of the time constant of the exponential distribution of substate events. The bimolecular rate constant for BPTI association was calculated from the reciprocal of the time constant of the exponential distribution of inter-substate events with an appropriate correction for missed events (*29*), divided by the BPTI concentration.

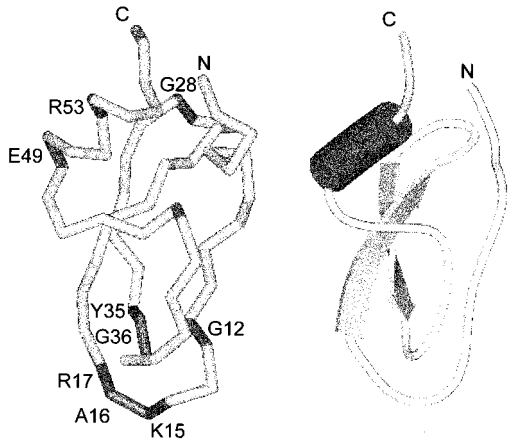

FIGURE 1: α-Carbon tracing of the peptide backbone of BPTI (left) with highlighted locations of various mutations investigated in this work. The view on the right is a corresponding diagram of α-helical (cylinder) and antiparallel β-strand (arrows) secondary structure. The figure was made with WebLab ViewerPro software from Molecular Simulations Inc. (San Diego, CA) using a crystal structure of BPTI (5pti) in the Brookhaven protein database.

Table 1: Fit Parameters for a 2-State Model of I-V Rectification for BPTI-Induced Substates[a]

BPTI or mutant	$K_0 \pm$ SE	$z' \pm$ SE
BPTI	0.62 ± 0.01	0.55 ± 0.01
G12D	0.61 ± 0.03	0.45 ± 0.02
K15V	1.65 ± 0.09	0.41 ± 0.03
K15F	0.16 ± 0.01	0.28 ± 0.01
K15G[b]	1.63 ± 0.06	0.43 ± 0.02
A16T	0.95 ± 0.04	0.67 ± 0.02
G28K	0.44 ± 0.02	0.62 ± 0.03
Y35D	0.90 ± 0.03	0.58 ± 0.02
G36D	0.72 ± 0.03	0.58 ± 0.02
E49A	0.79 ± 0.03	0.52 ± 0.02
R53A	0.94 ± 0.03	0.64 ± 0.02
K15V, R17L, desP2	1.94 + 0.04	0.37 + 0.01

[a] I−V data at 10 mV intervals from −50 to +50 mV for BPTI-induced substate currents were fit to a simple model of a two-state voltage-dependent equilibrium using eqs 1 and 2. Parameters describing the fits (K_0, z') are listed with error estimates (SE) derived from the fitting procedure. [b] This mutant exhibits two modes of inhibition, complete block and a less frequent substate. The fit refers to the substate.

RESULTS

Inhibitory Activity of 11 BPTI Variants on Single BK_{Ca} Channels. The tertiary structure of BPTI is illustrated in Figure 1(left) as an α-carbon tracing of the peptide backbone with marked locations of residues pertinent to this work. Also shown (Figure 1, right) is the schematic location of two prominent features of BPTI secondary structure consisting of a pair of twisted antiparallel β-strands (residues 17−25 and 29−36) and a C-terminal α-helix (residues 48−56). BPTI forms an extremely stable trypsin complex with an equilibrium dissociation constant of 6×10^{-14} M (*30*). In the crystal structure of the trypsin−BPTI complex, the primary binding loop formed by residues 11−19 of BPTI occupies the active-site cleft of trypsin and an adjacent loop of BPTI (residues 34−39) makes secondary contact (*31*−*33*). In this study, we compared the activity of native BPTI with 1 mutants listed in Tables 1 and 2. Note that these mutations involve substitutions of four residues in the primary trypsin contact loop (G12, K15, A16, and R17) and two in the secondary contact loop (Y35 and G36). In

Table 2: Kinetic Parameters for Binding of BPTI Mutants at +20 mV Measured from Dwell Times of Discrete Substate and Intersubstate Events

BPTI or mutant (net charge)	association rate k_{on} (10^5 s^{-1} M^{-1})	dissociation rate k_{off} (s^{-1})	equilibrium constant K_D (μM)	n
BPTI (+6)	46 ± 5	3.3 ± 0.4	0.73 ± 0.06	6
G12D (+5)	6.2 ± 0.9	4.3 ± 0.1	7.2 ± 1.0	3
K15V (+5)	2.3 ± 0.5	3.2 ±0.4	19 ± 5	6
K15F (+5)	0.79 ± 0.15	0.64 ± 0.09	4.6 ± 1.9	6
K15G (+5)[a]	3.5 ± 0.2	0.85 ± 0.12	2.4 ± 0.4	6
A16T (+6)	49 ± 3	3.9 ± 0.5	0.82 ± 0.09	3
G28K (+7)	32 ± 3	1.5 ± 0.4	0.44 ± 0.10	4
Y35D (+5)	9.2 ± 0.1	6.1 ± 1.1	7.8 ± 0.1	2
G36D (+5)	8.2 ± 1.0	8.8 ± 1.0	11 ± 2	3
E49A (+7)	120 + 30	2.5 ± 0.8	0.21 ± 0.02	2
R53A (+5)	8.5 ± 0.7	1.6 ± 0.3	1.9 ± 0.4	5
K15V, R17L, desP2 (+4)	0.25 ± 0.01	1.1 ± 0.1	44 ± 1	3

[a] Rate constants are computed for the blocked state induced by K15G.

addition, three mutations at the opposite end of the BPTI molecule were examined, one in the β-turn (G28) and two in the C-terminal α-helix (E49 and R53).

Figure 2 shows representative segments of single-channel records of BK_{Ca} from rat skeletal muscle incorporated into planar lipid bilayers and recorded at +20 mV in the presence of native BPTI and eight mutants. In the absence of BPTI (e.g., Figure 3, top trace), single BK_{Ca} channels normally fluctuate between two conductance levels corresponding to zero current at the closed state and ~220 pS at the open state. In the present experiments, high Ca^{2+} (>200 μM) on the intracellular side activates BK_{Ca} channel gating such that the probability of opening is > 0.90. Under these conditions, the majority of normal gating events are brief closing transitions (<50 ms) from the open state. BPTI binding to the channel results in the appearance of an intermediate current level or substate at ~30% of the open state current with a mean duration of 0.3 s at +20 mV. Kinetic analysis of such data has shown that the pattern of substate and intersubstate events reflects dwell times of BPTI-bound and unbound states, respectively (*16*, *29*).

The data of Figure 2 represent mutants that behave like native BPTI with respect to BK_{Ca} inhibition. These traces were selected to include rare examples of complete closures in order to identify the closed current level as marked with a dashed line. This comparison shows that the following mutants induce substates with a similar current amplitude (~30%) and mean duration (~0.1−0.6 s) at +20 mV: A16T, E49A, G12D, G28K, G36D, R53A, and Y35D. This result indicates that mutations involving charge changes at six different residues do not strongly perturb the BK_{Ca} interaction. However, it must be noted that all of these particular mutants also retain high affinity for trypsin as confirmed in trypsin inhibition assays.

We reasoned that if the interaction of BPTI with BK_{Ca} resembles the molecular interaction with trypsin, then mutations of BPTI that perturb trypsin inhibitory activity might also affect the BK_{Ca} interaction. Along these lines, we tested a triple mutation of BPTI (K15V, R17L, desP2) that was originally designed as a potent inhibitor of elastase and a poor inhibitor of trypsin. Enhancement of affinity for elastase is known to be favored by the K15V mutation (*20*, *34*). The Lys15 residue of BPTI confers specificity toward

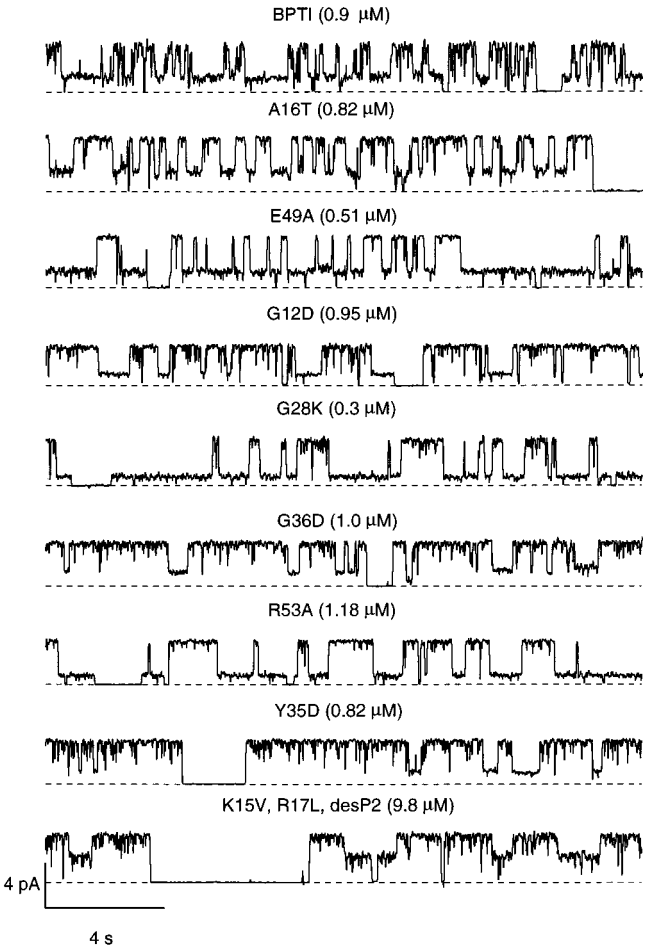

FIGURE 2: Comparison of subconductance behavior induced by native BPTI with that of various mutants. The top record shows typical behavior of a single BK_{Ca} channel recorded at +20 mV in the presence of 0.9 μM internal BPTI. The bottom eight records illustrate subconductance behavior produced by various BPTI mutants at the indicated internal concentration. Note that the relative substate current in the bottom record for the K15V, R17L, desP2 variant of BPTI is larger than that of the other records. The dashed line marks the closed state.

trypsin, a SerP that preferentially cleaves after Lys and Arg residues. Elastase generally cleaves after aliphatic residues, and substitution of Val for Lys15 apparently provides a favorable interaction of this side chain with the elastase specificity pocket. We found that this elastase inhibitor had the lowest affinity for the BK_{Ca} channel of all the mutants tested, primarily due to a slow association rate constant (Table 2). However, it also exhibited an interesting change in substate current amplitude. At +20 mV, the average level of the substate current for the triple mutant is ~60% of the open state compared to ~30% for native BPTI (e.g., Figure 2, bottom trace).

Since this observation pointed to an interaction between the most important SerP specificity residue of BPTI and the BK_{Ca} channel, we investigated three other BPTI mutants with residue replacements at Lys15: K15F, K15V, and K15G. As illustrated by the current records of Figure 3, these three mutants also exhibited significant changes in the amplitude of substate events. The Phe substitution of K15F resulted in a lower amplitude substate current corresponding to 10% of the open state at +20 mV and a longer mean duration of the substate (1.6 s for K15F vs 0.3 s for BPTI at +20 mV).

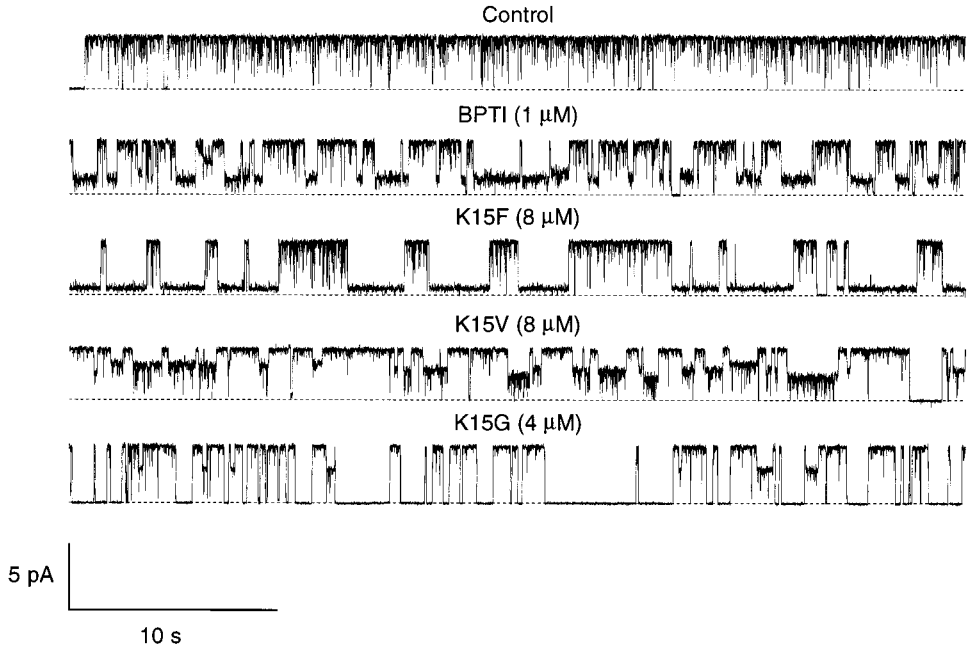

FIGURE 3: Three different substitutions of the K15 residue of BPTI produce different alterations in substate behavior. The top two records display typical current behavior of a single BK_{Ca} channel at +20 mV in the absence (Control) or presence of 1 μM native BPTI. Substitution of K15 by a Phe residue (K15F) or a Val residue (K15V) produces a smaller or larger substate level than native BPTI, respectively. The bottom record shows that the K15G mutation produces both complete blocking events and less frequent substate events of relatively short duration.

Unexpectedly, the Gly mutation, K15G, yielded a BPTI derivative that produced complete blocking events of relatively long duration (mean = 1.2 s at +20 mV) at a current level indistinguishable from the closed state of the channel (Figure 3, bottom trace). This same derivative also induced a different class of short-lived substate events at ~55% of the open state that occurred much less frequently than the complete blocking events. Apparently, the two types of discrete events induced by K15G are independent and do not interconvert kinetically as shown by the virtual absence of transitions from the 55% substate to the fully blocked level and vice versa (e.g., Figure 3, bottom trace). These two inhibitory modes cannot be easily explained by impurities or heterogeneity of the K15G sample since it was purified as a single peak on reversed-phase HPLC. As one possibility, we speculate that substitution of Lys15 by Gly may enhance backbone flexibility in BPTI allowing this particular mutant to bind to the channel in two different stable conformations, corresponding to either complete or partial inhibition of single-channel current.

Figure 3 also shows that the substate current level induced by the K15V mutant at ~55% of the open state is similar to that of the triple mutant elastase inhibitor in Figure 2 (bottom trace). This confirms the functional importance of the Val substitution at K15 relative to the substitution of Leu at R17 and deletion of a Pro residue near the N-terminus in the triple mutant.

Mean Current−Voltage Relationships of Substates Induced by BPTI Mutants. Previous work on single BK_{Ca} channels showed that the "substate" current induced by native BPTI is actually due to rapid fluctuation of the channel between the open state and a nearly closed state when the inhibitor is bound (*21*). The magnitude of the substate current induced by BPTI is also independent of the concentration of the inhibitor (*16*), a feature that distinguishes this phenomenon from a fast-blocking reaction such as that mediated by small organic cations such as tetraethylammonium. The appearance of a stable subconductance level in the presence of BPTI arises from the relationship between the kinetics of rapid pore fluctuations and the level of low-pass filtering used to resolve channel-gating events from high frequency background noise. In this work, we typically filtered BK_{Ca} channel records at 100 Hz, which is sufficient to adequately resolve mean current levels and substate dwell times but does not reveal the excess noise or rapid gating underlying substate events. BPTI-induced substates are also characterized by an intrinsic voltage dependence which gives rise to an inwardly rectifying current−voltage (I−V) relationship. This behavior is illustrated in Figure 4, panels B−D, where typical I−V data for the open state and BPTI-induced substates are plotted for comparison.

An example of how of substate I−V rectification differs for native and mutant BPTI molecules is shown in Figure 4A. This figure compares the single-channel behavior of native BPTI with the triple mutant at +50 mV. At his voltage, the substate current for native BPTI is ~17% of the open state vs ~48% for the triple mutant. Thus, the difference in the relative substate current of the two inhibitors at +50 mV is even more pronounced than that at +20 mV (Figure 2). To document this behavior, we analyzed mean substate I−V relationships in the range of −50 to +60 mV for all of the BPTI mutants.

Typical I−V data for the open state and substate of native BPTI and two mutants, G28K and Y35D, are shown in Figure 4B. The open channel I−V relation is linear between −50 and +60 mV, corresponding to an ohmic conductance that falls in the range of 180−220 pS under these conditions (symmetrical 50 mM KCl, 10 mM Mops-KOH, pH 7.4). The comparison of Figure 4B shows that the substate I−V curves of the G28K and Y35D mutants are nearly indistinguishable

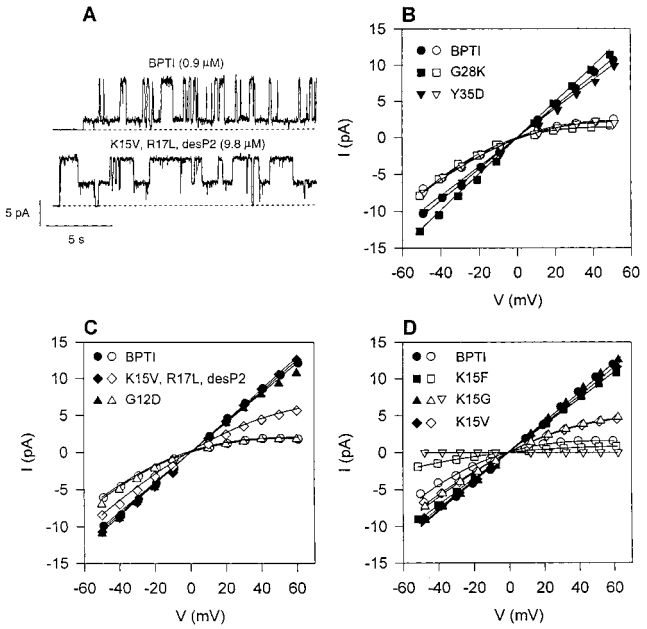

FIGURE 4: Comparison of current−voltage (I−V) behavior of open state and substate events of single BK_{Ca} channels recorded in the presence of native BPTI or various BPTI mutants. (A) Records of a single BK_{Ca} channel at +50 mV in the presence of either native BPTI or the triple mutant, K15V, R17L, desP2, reveal a large difference in the substate current level. (B, C, D) Single-channel I−V curves of the open state (closed symbols) or subconductance state (open symbols) of typical BK_{Ca} channels measured in the presence of selected BPTI mutants are compared with that of native BPTI as indicated by symbol legends. Solid lines for open state I−V data are simple linear regression fits to nearly ohmic behavior. Solid lines for the rectifying substate I−V curves are fits to a Boltzmann function of voltage (eqs 1 and 2).

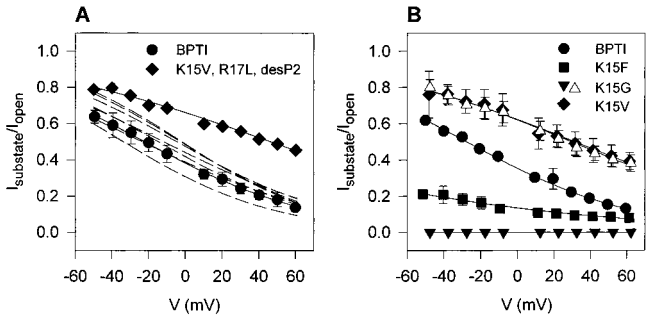

FIGURE 5: Comparison of rectification ratio vs voltage for native BPTI and mutants. I−V data is plotted as the ratio of substate current to open state current as a function of voltage for native BPTI and mutations involving K15 as indicated by the symbol legends in panels A and B. Solid lines are fit to a Boltzmann function of voltage (eqs 1 and 2). In panel A, the dashed lines close to the native BPTI data are Boltzmann fits for the following 7 mutants: G12D, A16T, G28K, Y35D, G36D, E49A, and R53A. Data points for these latter mutants are not shown for sake of clarity. Parameters for the fits are listed in Table 1.

from native BPTI. Likewise, I−V data for another mutation outside the primary trypsin contact loop, G12D, is also superimposable with that of native BPTI as shown in Figure 4C. However, the substate I−V relation for the triple mutant plotted in Figure 4C exhibits a larger current than native BPTI at all voltages. In contrast, I−V data for the K15F mutant plotted in Figure 4D is shifted to lower current than that of BPTI. Figure 4D also shows that the high-conductance substate induced by the K15G mutant exhibits similar behavior to the K15V mutant while the zero current level induced by K15G is unchanged at all voltages in this range.

The rectification behavior of the various BPTI mutants can be compared more directly by examining the ratio of substate to open channel current as a function of voltage. Such plots are shown in Figure 5 where the mean current ratio for 2−5 single channels is plotted for native BPTI and various mutants in the voltage range of −50 to +60 mV. The data are fit to a two-state model of voltage-dependent rectification based on a Boltzmann function of voltage as described in the Experimental Procedures (eqs 1 and 2). Figure 5A compares the substate current ratio of wild-type BPTI with that of seven BPTI mutants which do not contain a mutation at K15 and one which does, the triple mutant (K15V, R17L, and desP2). To avoid overlapping data points, only dotted lines corresponding to best fits of the Boltzmann function (eqs 1 and 2) are shown for the following mutants: G12D, A16T, G28K, Y35D, G36D, E49A, and R53A. This comparison shows that the substate current ratio of the latter seven BPTI mutants is practically the same as native BPTI, whereas that of the triple mutant is distinctly larger over the tested voltage range. Figure 5B also clearly shows an enhanced current ratio at all voltages for K15V and the substate of K15G, in contrast to a decreased current ratio at all voltages for K15F and the zero current state of K15G.

The fits of Figures 4 and 5 also demonstrate that the two-state fluctuation model provides a good description of the I−V rectification behavior of the various BPTI mutants, except for the complete block by the K15G mutant. In this model, the substate current ratio is a function of two parameters, K_0 and z' (*21*). K_0 is a zero-voltage equilibrium constant expressed as the ratio of the probability of the channel occupying the open state to that of the closed state at 0 mV for the rapid gating process that underlies the substate. The second parameter, z', is equivalent to the apparent "gating charge" of the rapid voltage-dependent fluctuation, where a value of $z' = 1.0$ corresponds to a reaction that senses the equivalent of one charge moving across the whole transmembrane electric field. Parameters obtained from fitting data to this model are summarized in Table 1. The results indicate that mutations at K15 affect the K_0 equilibrium constant of the underlying flickering process by shifting it to lower values (K15F, $K_0 = 0.16$; K15G, $K_0 = 0$) or higher values (triple mutant, $K_0 = 1.94$; K15V, $K_0 = 1.65$; K15G, $K_0 = 1.63$) than that of BPTI and the other non-K15 mutations (range of $K_0 = 0.44-0.95$). In contrast, Table 1 shows that relative changes in the z' parameter of K15 mutants are not as large as those of K_0.

Dissociation and Association Rate Constants for BPTI Mutants. Previous work has shown that the interaction of BPTI with BK_{Ca} channels is well described by a reversible binding reaction at one site or a kinetically homogeneous class of sites (*16*, *29*). This conclusion is based on (1) monoexponential distributions of dwell time histograms of substate and inter-substate events, (2) independence of the mean substate dwell time with respect to BPTI concentration, and (3) a reciprocal relationship between the intersubstate dwell time and BPTI concentration. These relationships are diagnostic features of a simple binding and unbinding process governed by a bimolecular association rate constant (k_{on}) and a first-order dissociation rate constant (k_{off}). These rate constants were measured for the various BPTI mutants at

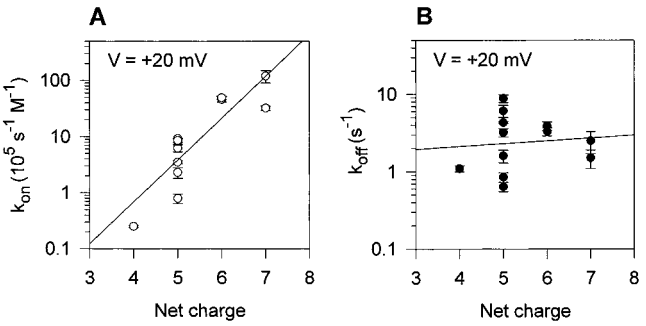

FIGURE 6: Effect of various mutations on binding kinetics of BPTI. Association (A) and dissociation (B) rate constants of BPTI and various mutants were measured from dwell time histograms of substate events at +20 mV and plotted vs net charge of the BPTI variant. Solid lines correspond to linear regression fits of the logarithm of the rate constant vs net charge.

+20 and +50 mV using dwell time histograms as described previously (*29*).

The kinetic results at +20 mV listed in Table 2 show that the mutations studied here resulted in modest changes of k_{off}. Two mutations that led to a perceptibly faster dissociation rate than native BPTI were Y35D and G36D located in the secondary trypsin contact loop, but this enhancement only amounted to factors of 1.4−1.8-fold for Y35D and 2.3−2.7-fold for G36D, with the range cited for data collected at +20 and +50 mV. Several of the mutations actually stabilized the bound complex, as indicated by a slower rate of dissociation than native BPTI. In particular, the K15F mutant exhibited a 5−8-fold longer substate dwell time (i.e., the reciprocal of k_{off}) than BPTI itself. The apparent blocked state induced by K15G was also 4−9-fold longer than the mean duration of the BPTI substate. This implies that the amino acid side chain at the K15 position can affect the lifetime of the BPTI−channel complex, while it also determines the amplitude of the substate current. On the basis of these results, it appears several residues in the secondary and primary trypsin-binding loops of BPTI do significantly affect the interaction with the BK_{Ca} channel. However, when interpreting these data, we must consider that such changes in k_{off} are rather small in comparison to rate enhancements of >100-fold that have been observed in other examples of critical residues that lie within the binding surface of toxin-channel or inhibitor−enzyme complexes (*35*, *36*).

Larger effects of the mutations are observed for the k_{on} rate constants, particularly for residue substitutions that involve charge changes. This point is illustrated in Figure 6, which shows the measured rate constants plotted as a function of net charge of the BPTI mutant. The k_{on} value exhibits a tendency to increase with net positive charge as shown by a positive correlation between the logarithm of k_{on} and net charge (Figure 6A). The correlation coefficient, r, for linear regression of $\ln(k_{on})$ vs net charge is +0.86 for the data at +20 mV and +0.82 at +50 mV (not shown). In contrast, the k_{off} data plotted in Figures 6B do not show a significant correlation with net charge ($r = 0.095$ at +20 mV, $r = 0.16$ at +50 mV). These results indicate that the association rate of BPTI at the internal side of the BK_{Ca} channel is controlled by a long-range electrostatic interaction. This finding is not unexpected, since the magnitude of the BPTI association rate constant was previously found to be very sensitive to ionic strength (*16*).

For binding of a point charge of valence z to a charged surface, the association rate constant would be expected to follow a Boltzmann relationship with respect to the surface potential, Ψ:

$$k_{on} = k_{on}^{0} \exp(-z\psi F/RT) \qquad (3)$$

where k_{on}^{0} is the intrinsic association rate constant at zero surface potential and RT/F equals 25.4 mV at 22 °C (*37*). Since a protein as large as BPTI is a poor approximation of a point charge, eq 3 is not expected to be quantitatively valid. However, the estimate of Ψ obtained by fitting the data of Figure 6A to eq 3 is useful for comparison with other examples where a similar relationship has been described in the literature. Here, we obtain $\Psi = -43$ or -42 mV for the apparent surface potential calculated for data at +20 and +50 mV, respectively. This is larger than the value of $\Psi = -13$ mV at 250 mM KCl obtained for the blocking interaction of a series of ball peptide homologues with an intracellular site on BK_{Ca} from pig coronary artery (*38*). Similar work with another series of ball peptide homologues yielded $\Psi = -23$ mV at 140 mM KCl for internal block of the *Shaker* K^+ channel (*39*). A value of Ψ close to that observed here (−43 mV) was also observed for the interaction of charged derivatives of saxitoxin with a binding site on the extracellular side of skeletal muscle Na^+ channels studied at 0.2 M NaCl (*37*). These examples illustrate that local negative surface charge is an important factor in ligand interactions with cation-selective ion channels at both internal and external binding sites.

Another noteworthy feature of the interaction of BPTI with BK_{Ca} is that the k_{on} value for native $BPTI^{+6}$ is relatively low (4.6×10^6 s^{-1} M^{-1} at +20 mV and 50 mM KCl) compared to the fastest diffusion-limited association rate constant for a ligand−protein interaction, expected to be in the range of $\sim 10^9 - 10^{10}$ s^{-1} M^{-1} (*40*). Considering that the observed association rate for $BPTI^{+6}$ has a large built-in enhancement due to the attractive electrostatic interaction, it is clear that this ligand must overcome a substantial energy barrier in going from solution to the bound state in the absence of surface charge effects. As an illustration, if the logarithmic relationship between k_{on} and net charge observed in Figure 6A is extrapolated to $z = 0$, one finds a very low intrinsic association rate of $k_{on}^{0} \approx 72$ s^{-1} M^{-1}. Thus, for a BPTI mutant with zero net charge or in the absence of a local surface potential, one would expect an immeasurably low affinity. This deduction is consistent with a result we have obtained with another homologue of BPTI.

A Kunitz inhibitor domain (KID) occurs naturally in certain alternatively spliced variants of amyloid β-protein precursor (APP). Proteolytic degradation of APP leads to the production of amyloid β-protein that is present in amyloid deposits in the brains of patients with Alzheimer's disease (*41*). As shown in Figure 7, KID has a modest level of overall sequence identity with BPTI (~43%). However, within the primary and secondary trypsin contact loops, the two proteins are almost identical with only four nonconservative substitutions. The peptide backbone fold of KID is also very similar to that of BPTI (*25*, *26*). Furthermore, KID is known to be a potent inhibitor of trypsin with a K_i of 10^{-10} M (*27*). We used the planar bilayer assay to test the effect of KID on BK_{Ca}. The hypothesis of a SerP-like domain in the BK_{Ca}

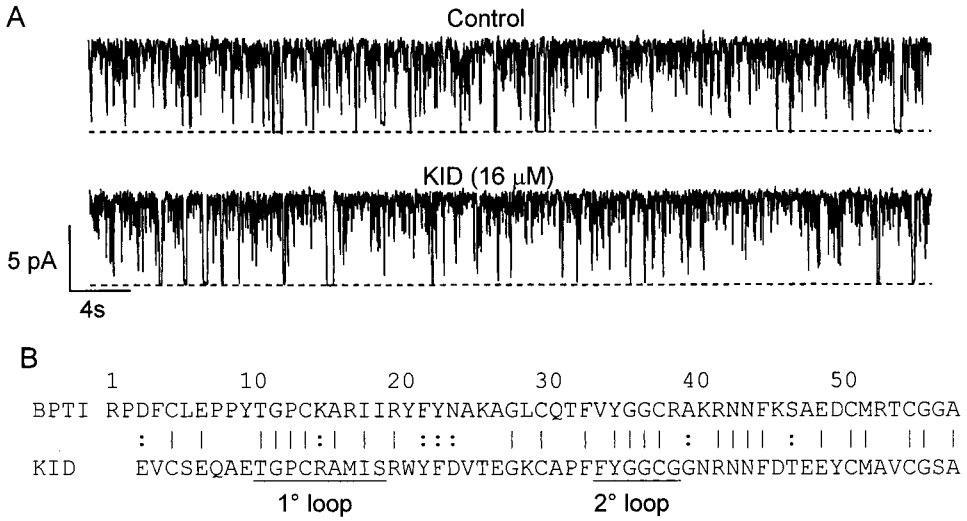

FIGURE 7: Experiment showing that the Kunitz inhibitor domain (KID) of amyloid β-protein precursor is inactive in the production of substate events. (A) Representative behavior of a single rat muscle BK_{Ca} channel as recorded in a planar bilayer before and after addition of 16 μM KID to the chamber corresponding to the intracellular side of the channel. The dashed line indicates the zero-current or closed level. Holding voltage: +30 mV. (B) Sequence alignment of BPTI and KID showing identical (solid line) and conservative (dotted line) substitutions.

channel (*18*) predicts that KID ought to be active in the production of substate events. However, we did not observe substate events or any inhibitory effect of KID at concentrations up to 16 μM on the internal side of single BK_{Ca} channels (Figure 7A). This result can be explained by the fact that KID has a net charge of −4 compared to +6 for BPTI (see sequence comparison of Figure 7B). On the basis of extrapolation of the steep relationship between k_{on} vs net charge observed for BPTI mutants (Figure 6A), a homologue of BPTI with a negative net charge would not be expected to have detectable activity at an experimentally accessible concentration, due to an extremely low rate of association.

DISCUSSION

Role of Electrostatics and Identification of an Inhibitor Residue in the Contact Site of BPTI and the BK_{Ca} Channel. A major objective of this work was to identify residues of BPTI that are located in the contact surface for binding to BK_{Ca}. In selecting mutants, we assumed that changes in the charge of side chains would be likely to produce the strongest perturbations of binding kinetics. Another important consideration was preservation of native structure so that observed mutational effects reflect a change in a specific protein−protein interaction and not the misfolding of BPTI. For this reason, we studied a number of previously described mutations of BPTI and relied on their ability to inhibit trypsin as an indicator of native structure. The tested mutants involved either substitution of a neutral side chain with a negatively charged one (G12D, Y35D, and G36D), substitution of a neutral side chain with a positively charged one (G28K), or neutralization of a charged residue (E49A, R53A, R17L, K15G, K15V, and K15F). One of the tested mutants, A16T, did not involve a change in charge. This latter molecule exhibited practically indistinguishable activity from native BPTI (Tables 1 and 2). Residues 11−19 in the primary trypsin contact loop of BPTI were of particular interest for evaluating whether this region is a recognition site for BK_{Ca}.

We found that all of the tested mutants are active in the production of discrete substates with relatively modest changes in k_{on} and k_{off}. This may mean that we have not yet identified the location of key residues required for this protein−protein interaction. Alternatively, we may be dealing with an example of intermolecular recognition where the contribution of any particular amino acid side chain to the binding energy is relatively minor compared to intermolecular shape complementarity and peptide backbone interactions of the contact surfaces. This latter explanation actually describes the essential basis for molecular recognition of many natural proteinase inhibitors by SerP enzymes (*42*−*44*). We argue below that the results described here are consistent with this type of interaction.

One of the major conclusions from this study is that surface charges of BPTI have a strong influence on the magnitude of the inhibitor association rate constant. As mentioned above, electrostatic interactions are known to be an important factor in the blocking interactions of positively charged ball peptide homologues on the intracellular side of BK_{Ca} channels (*38*, *39*). In this case, the net charge of the ball peptide homologue and internal ionic strength both influence the association rate constant in a manner expected for a strongly attractive charge−charge interaction. Likewise, the ionic strength dependence of the association rate constant of BPTI binding to the BK_{Ca} channel is very steep, with k_{on} increasing ~1000-fold for a 10-fold decrease in the internal ionic strength (*16*). The present observation of a positive correlation between between k_{on} and the net charge of BPTI undoubtedly reflects an attractive interaction between positive surface potential of the inhibitor and a region of negative surface potential somewhere on the channel protein.

A possible location of negative surface charge density on BK_{Ca} is a particular conserved sequence in the C-terminal region that contains one Glu and seven Asp residues within a short stretch of 11 continuous amino acids. This sequence has been termed "the calcium bowl" based on the observation that mutations in this region affect the Ca^{2+} dependence of activation (*6*). The negatively charged calcium bowl motif is actually located within a ~250 residue sequence near the C-terminus of the α-subunit of the BK_{Ca} channel that we

have previously proposed to be homologous to the family of SerP enzymes (*18*). The location of the calcium bowl sequence in an alignment with the SerP family corresponds to the location of a known Ca^{2+}-binding loop in certain proteinases such as trypsin, elastase, and coagulation factors IX and X (*45*, *46*). Binding of $BPTI^{+6}$ to the SerP-like domain may involve diffusion of the basic protein inhibitor within close proximity to this highly anionic region on the BK_{Ca} channel, thus accounting for a part of the strongly attractive electrostatic interaction. Repulsive electrostatic interactions between positively charged Kunitz inhibitor molecules or between a Kunitz inhibitor and a basic ball peptide have also been proposed to influence the kinetics of negatively coupled binding equilibria that have been characterized on the intracellular side of the BK_{Ca} channel (*29*).

The second major conclusion of this study is that the chemical nature of the side chain at the K15 residue position of BPTI is a major determinant of the mean current and current−voltage relationship of the apparent subconductance state induced by BPTI. This observation provides new information relevant to the location of the contact region and the mechanism of substate production. The notion that the substate current must depend on the structure of the Kunitz inhibitor was anticipated from previous experiments comparing the action of BPTI with DTX-I, a homologue of BPTI found in venom of the black mamba snake, *Dendroaspis polylepsis* (*16*). DTX-I is a member of a subfamily of Kunitz domain proteins called dendrotoxins, some of which are potent inhibitors of voltage-gated K^+ channels at an *extracellular* site. However, DTX-I produces long-lived subconductance states in BK_{Ca} by binding to an *intracellular* site that also binds BPTI (*16*, *29*). This is intriguing since there is only 32% sequence identity between BPTI and DTX-I, although they exhibit a very similar tertiary fold of their respective peptide backbones (*47*). In addition, the mean current of the substate induced by BPTI and DTX-I is quite different, ∼30% vs ∼70% of the open state current at +20 mV for BPTI and DTX-I, respectively (*21*). This implies that there is a specific relationship between the structure of the Kunitz inhibitor and the mean substate current that is produced. Here we have demonstrated that the structural element of BPTI that determines this change in the effective single-channel conductance of BK_{Ca} may involve protein mass as little as one side chain at the K15 position. Although we have so far studied only three residue substitutions, V, F and G, in place of K15, these replacements result in a substate that is either 0% (K15G), ∼10% (K15F), ∼30% (K15 wild-type), or ∼55% (K15V and K15G) of the open state current at +20 mV (Figure 5B). The simplest explanation of how a single residue can have such a profound effect on single-channel conductance must start with the assumption that the K15 residue is located close to the channel surface in the bound state. This finding therefore implies that K15 is a contact residue for the BPTI−BK_{Ca} binding interaction.

Comparison to the Interaction of Proteinase Inhibitors and SerP Enzymes: A Proposed Mechanism for the Substate Effect. In view of the fact that K15 mutations implicate the primary trypsin contact loop as a site of interaction with BK_{Ca}, it is pertinent to ask if there are other similarities to the interaction of BPTI with SerP enzymes. An often noted feature of BPTI is its ability to inhibit a variety of divergent SerP homologues over a wide range of affinity. For example, BPTI inhibits bovine trypsin with very high affinity K_D of 6×10^{-14} M, but it also inhibits the following SerPs with lower affinity: chymotrypsin (9.5×10^{-9} M), kallikrein (8.4×10^{-10} M), plasmin (1×10^{-9}M), thrombin (4×10^{-5} M), and urokinase (2×10^{-5} M), with respective K_Ds given in parentheses (*48*−*50*). BPTI is also able to recognize and bind to catalytically inactive SerP precursors such as trypsinogen ($K_D = 2 \times 10^{-6}$ M) (*51*, *52*), a chemically inactivated trypsin derivative such as anhydrotrypsin ($K_D = 1.1 \times 10^{-13}$ M) (*53*), and an inactive SerP homologue such as human heparin binding protein/azurocidin ($K_D = 1 \times 10^{-7}$ M) (*49*). This listing of SerP interactions includes several examples of affinities in the range observed here (Table 2).

A variety of crystallographic analyses have determined that the essential basis for the binding interaction between BPTI and diverse SerP targets is the formation of a short stretch of antiparallel β-sheet between the N-terminal end of the primary contact loop of the inhibitor (BPTI residues 13−15) with a complementary region of peptide backbone involving several residues near the C-terminus of the SerP enzyme (chymotrypsin residues 214−216, 193, and 193) (*31*, *33*). In addition, there is tight shape complementarity between the binding surface of BPTI (∼700 Å^2) and the SerP-binding cleft, such that water is essentially excluded from the protein−protein interface (*44*). Other than the special interaction of the Lys15 side chain of BPTI, which makes a specific electrostatic interaction with Asp189 in the substrate specificity pocket of trypsin, there are no specific side-chain interactions that are required for molecular recognition between BPTI and SerPs. This situation is reflected in the results of alanine-scanning mutagenesis of the inhibitor contact region of BPTI (scanned residues 11−20 and 33−39), which found mostly rather modest changes in the binding constants of 15 Ala mutants of BPTI assayed against trypsin and chymotrypsin (*42*). For example, the K15A mutation of BPTI only reduced the affinity for chymotrypsin by 30-fold and increased the BPTI dissociation rate constant by 11-fold. Such small effects of substitution of individual side chains on binding affinity are evocative of the results found here, which indicate affinity changes less than 26-fold for the interaction of a collection of BPTI point mutants with BK_{Ca}.

The essential features of the binding interaction with SerPs summarized above provide a plausible basis for interpreting results obtained for the channel interaction. In a previous study, we described a proposed alignment of SerP sequences with the putative SerP-like domain of *Drosophila* and mammalian BK_{Ca} channels (*18*). The significance of this alignment is based on identification by sequence similarity of a number of potential β-strand structural elements common to all SerPs and the presence of an acidic sequence (the calcium bowl motif) at the corresponding location of a Ca^{2+}-binding loop in certain SerPs. This alignment predicts that the putative SerP domain in the BK_{Ca} channel is catalytically inactive due to substitution of residues corresponding to His57 and Asp102 of chymotrypsin. This domain may nevertheless adopt a SerP-like tertiary fold and bind BPTI with a relatively low affinity based on the analogy of other inactive SerP homologues described above. In this case, mutation of BPTI residues would be expected to have small effects on binding energy if main-chain hydrogen-bonding dominates the binding interaction. In such a protein complex,

the Lys15 side chain of BPTI may lie outside the subsite corresponding to the P1 specificity pocket of SerPs, as found in the crystal structure of BPTI bound to chymotrypsin (*32*, *48*). This is in contrast to the classic conformation of the BPTI−trypsin complex where the Lys15 side chain is situated within the P1 pocket where it interacts with Asp189 (*33*, *54*). In this scenario, the dependence of the substate phenomenon in the BPTI−BK_{Ca} interaction on residue substitutions of Lys15 could be explained by conformational changes in the SerP-like domain of BK_{Ca} that are triggered by BPTI binding. A precedent for such inhibitor-induced conformational changes in SerPs has been described for BPTI binding to trypsinogen, where the active site is initially disordered but is converted to a trypsin-like conformation upon binding of the inhibitor (*55*).

On the basis of available evidence, the subconductance effect induced by BPTI is due to a rapidly flickering process that involves a conformational change transmitted from the inhibitor binding site to the channel pore (*21*). This implies that BPTI binding induces an instability in the gating process. Recent studies of BK_{Ca} gating have concluded that Ca^{2+}-binding is coupled to the movement of an S4 voltage sensor in each subunit of the homotetramer (*56*, *57*). Since BPTI essentially binds to one subunit at a time in the homotetramer (*29*), this would produce a conformational change that disrupts one BK_{Ca} channel subunit out of four that cooperate in opening the central channel. In effect, the binding of BPTI to one subunit of the tetramer would disrupt the oligomeric symmetry of the open state. Consequently, this disruption would perturb allosteric gating of the pore in a tetrameric complex. We surmise that the open state would be unstable in such a complex and the channel would tend to fluctuate rapidly between the open state and an abnormal closed state. We therefore suggest that the SerP-like domain in the BK_{Ca} channel is a Ca^{2+}-binding domain that engages in a direct interaction with the channel-forming domain. In this model, illustrated schematically in Figure 8, such a domain−domain interaction is modulated by Ca^{2+} binding and is proposed to favor the movement of the S4 voltage sensor to a permissive state for normal channel activation. We propose that this mechanism underlies the rapid flickering that leads to the appearance of a BPTI-induced subconductance state in single-channel records.

Comparison with Other Examples of Peptide Toxins That Induce Subconductance Events. Single-channel studies have uncovered other cases where peptide toxins induce subconductance events. One example is μ-conotoxin GIIIA, a cone snail peptide that blocks voltage-dependent Na^+ channels of skeletal muscle by binding to a site in the external vestibule. As observed in single Na^+ channels activated by batrachotoxin, μ-conotoxin GIIIA itself produces a complete block of the channel (*58*). However, an R13Q mutant of GIIIA results in an incomplete block corresponding to a discrete substate at 28% of the open channel current (*59*). Substitution of other residues at this position of μ-conotoxin results in a higher or lower substate current, depending on the chemical nature of the side chain (*60*). This behavior superficially resembles our observations with K15 mutations of BPTI; however, evidence suggests that it is mechanistically distinct. The R13 residue of GIIIA has been found to be located close, probably within a few angstroms of particular Na^+ channel residues that are known to line the outer pore entrance (*60*).

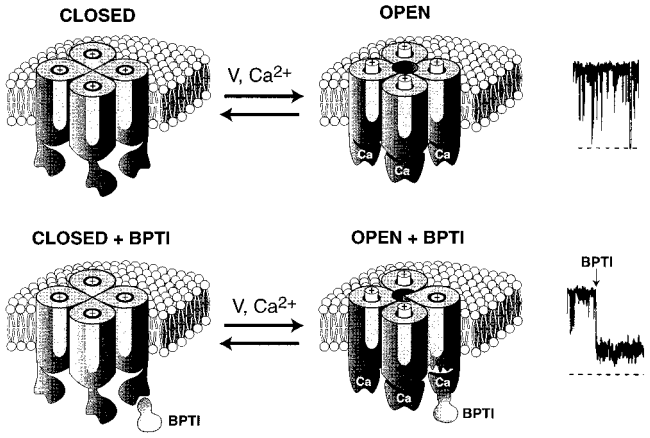

FIGURE 8: Schematic model of BK_{Ca} channel gating and proposed mechanism for substate production by BPTI. The top part of the sketch depicts various types of conformational changes proposed to occur with activation of channel opening by positive voltage and intracellular Ca^{2+}. In the closed state (left), S4 voltage sensing elements (small cylinders marked with +) in each of the subunits of the tetramer are positioned closer to the intracellular side of the membrane. Binding of Ca^{2+} to an intracellular site on the SerP-like domain enables this latter domain to interact more strongly with the transmembrane domain and lower the free energy required for outward movement of the S4 voltage sensors. This promotes an allosteric interaction between the subunits within the transmembrane region that leads to cooperative opening of the central channel. In the bottom part of the sketch, binding of BPTI to one of the SerP-like domains results in a conformation that does not allow normal movement of the voltage sensor in that subunit. Thus, one subunit out of four is frequently in a different conformation than the others and channel opening is destabilized. Such a BPTI-occupied channel rapidly fluctuates between the open state and a closed state of the pore. Low-pass filtering of the rapidly flickering current gives rise to the appearance of a low-conductance substate in the single-channel record.

In this location, the R13 residue of GIIIA is presumably close enough to the pore to exert a direct electrostatic effect on the conduction of permeant Na^+ ions. In contrast, in the case of BK_{Ca}, the internal inhibitor binding site appears to be located at some distance from the entrance to the inner pore, such that BPTI and DTX-I do not kinetically interfere with pore blockers such as Ba^{2+} and tetraethylammonium (*16*). However, the BPTI/DTX-I site on the BK_{Ca} channel does negatively interact with binding of a larger and more highly charged ball peptide homologue that also blocks the pore from the inside (*29*).

In another example, δ-dendrotoxin from the green mamba snake (*Dendroaspis angusticeps*) is an inhibitor of the ROMK1 inward rectifier K^+ channel that produces a residual 10% substate current when it is bound to the outer vestibule of this particular K^+ channel (*61*). Mutations have not yet been identified that modulate the level of this substate current. The subconductance state produced by binding of BPTI/DTX-I to the BK_{Ca} channel is also distinct from such examples of partial pore occlusion by peptide toxins, since it is not due to direct physical obstruction, but reflects a rapidly flickering gating transition as discussed above.

Possible Relationship of the BPTI-Binding Site to Inactivation Mediated by β-Subunits. "Ball peptide" is a 20-residue peptide that contains an excess of basic vs acidic residues and corresponds to a sequence at the N-terminus of the *Shaker* B K^+ channel of *Drosophila*. This region of

the *Shaker* channel is thought to function as a natural inactivating particle that mediates rapid channel inactivation after opening in response to voltage (*62*, *63*). Studies have shown that similar peptides are capable of blocking BK_{Ca} from the intracellular side (*38*, *64*), leading to the notion that both types of K^+ channels share a structurally related receptor site for such inactivation domains or ball peptides. However, it has been found that some vertebrate BK_{Ca}s exist as a complex with an accessory β-subunit (*65*). β-Subunits of BK_{Ca} channels comprise a multigene family, some of which produce BK_{Ca} channels with rapid inactivation when coexpressed with the channel-forming α-subunit (*66*, *67*). These latter studies have shown that a ball-peptide-like sequence at the amino terminus of such β-subunits mediate this inactivation process in a manner similar to that described for *Shaker* K^+ channels. However, in contrast to the ball peptide interaction with *Shaker*, the naturally tethered BK_{Ca} ball peptide of the β-subunit does not appear to be competitive with small intracellular pore blocking molecules such as $QX\text{-}314^+$, a triethyl-derivative of ammonium (*67*). This raises the possibility that the process of β-subunit-mediated inactivation in BK_{Ca} does not involve the same internally accessible pore-blocking site as that of small molecule blockers. As an alternative to direct block of the pore, it is possible that the N-terminal ball domain of the β-subunit acts at the same site as BPTI. Since we have observed that homologues of BPTI such as the K15G mutation are capable of inducing apparently complete blocking events, protein ligands such as ball domains could potentially induce long-lived closed states in BK_{Ca} by binding at the site of BPTI interaction. Functional studies are needed to assess whether the BPTI-binding site has any relationship to β-subunit-mediated inactivation in BK_{Ca}.

Summary. Measurements of the interaction of 11 BPTI mutants with single BK_{Ca} channels have revealed that the magnitude of the association rate constant for binding to an intracellular site on the channel is correlated with the number of positively charged surface residues of the inhibitor, as expected for an electrostatic interaction. The observation that mutations of Lys15 modulate the mean unitary current level of the BPTI-bound channel identifies this residue located within the trypsin inhibitory loop of BPTI as a contact region for the BK_{Ca} channel interaction. This finding and the relatively small effects of mutations on the inhibitor dissociation rate suggest that molecular recognition for this interaction may not be primarily based on side-chain interactions. Instead, it could involve complementary hydrogen bonding between short regions of the peptide backbone of the inhibitory loop and the channel, similar to the essential binding mechanism of BPTI to SerPs. Studies of this protein−channel interaction have led to a working model for the production of substate events that involves binding of one BPTI molecule to one of four putative SerP-like domains on the tetrameric channel complex. This association is proposed to result in an aberrant and rapidly fluctuating gating behavior that resembles a subconductance state under particular filtering conditions. Such unstable gating may result from disruption of tetrameric symmetry and perturbation of normal allosteric intersubunit interactions that occur in the open channel. The fact that the K15G mutant of BPTI produces an apparent blocked state of the channel also raises the question of whether the BPTI-binding site is involved in normal channel inactivation mediated by certain types of BK_{Ca} β-subunits.

ACKNOWLEDGMENT

We especially thank Dr. Paul P. Tamburini of Bayer Corp., West Haven, CT, for providing Kunitz inhibitors and many helpful discussion regarding their structure and activity.

REFERENCES

1. Moczydlowski, E. (1998) *Chem. Biol. 5*, R291−R301.
2. Gribkoff, V. K., Starrett, J. E., and Dworetzkey, S. I. (1997) *Adv. Pharmacol. 37*, 319−348.
3. Butler, A., Tsunoda, S., McCobb, D. P., Wei, A., and Salkoff, L. (1993) *Science 261*, 221−224.
4. Atkinson, N. S., Robertson, G. A., and Ganetzky, B. (1991) *Science 253*, 551−555.
5. Doyle, D. A., Cabral, J. M., Pfuetzner, R. A., Kuo, A., Gulbis, J. M., Cohen, S. L., Chait, B. T., and MacKinnon, R. (1998) *Science 280*, 69−77.
6. Schreiber, M., and Salkoff, L. (1997) *Biophys. J. 73*, 1355−1363.
7. Wei, A., Solaro, C., Lingle, C., and Salkoff, L. (1994) *Neuron 13*, 671−681.
8. Wang, J., Zhou, Y., Wen, H., and Levitan, I. B. (1999) *J. Neurosci. 19*, *RC4*, 1−7.
9. Xia, X., Hirschberg, B., Smolik, S., Forte, M., and Adelman, J. P. (1998) *J. Neurosci. 18*, 2360−2369.
10. Schopperle, W. M., Holmqvist, M. H., Zhou, Y., Wang, J., Wang, Z., Griffith, L. C., Keselman, I., Kusinitz, F., Dagan, D., and Levitan, I. B. (1998) *Neuron 20*, 565−576.
11. Ranganathan, R., Lewis, J. H., and MacKinnon, R. (1996) *Neuron 16*, 131−139.
12. Goldstein, S. A. N., Pheasant, D. J., and Miller, C. (1994) *Neuron 12*, 1377−1388.
13. Hidalgo, P., and MacKinnon, R. (1995) *Science 268*, 307−310.
14. MacKinnon, R., Cohen, S. L., Kuo, A., Lee, A., and Chait, B. (1998) *Science 280*, 106−109.
15. Lucchesi, K., and Moczydlowski, E. (1990) *Neuron 2*, 141−148.
16. Lucchesi, K. J., and Moczydlowski, E. (1991) *J. Gen. Physiol. 97*, 1295−1319.
17. Moss, G. W. J., Marshall, J., Morabito, M., Howe, J. R., and Moczydlowski, E. (1996) *Biochemistry 35*, 16024−16035.
18. Moss, G. W. J., Marshall, J., and Moczydlowski, E. (1996) *J. Gen. Physiol. 108*, 473−484.
19. Goldenberg, D. P., Berger, J. M., Laheru, D. A., Wooden, S., and Zhang, J.-X. (1992) *Proc. Natl. Acad. Sci. U.S.A. 89*, 5083−5087.
20. Krowarsch, D., Dadlez, M., Buczek, O., Krokoszynska, I., Smalas, A. O., and Otlewski, J. (1999) *J. Mol. Biol. 289*, 175−186.
21. Moss, G. W. J., and Moczydlowski, E. (1996) *J. Gen. Physiol. 107*, 47−68.
22. Coplen, L. J., Frieden, R. W., and Goldenberg, D. P. (1990) *Proteins: Struct., Funct., Genet. 7*, 16−31.
23. Goldenberg, D. P. (1988) *Biochemistry 27*, 2481−2489.
24. Kassel, B. (1970) *Methods Enzymol. 19*, 844−852.
25. Heald, S. L., Tilton, R. F., Hammond, L. J., Lee, A., Bayney, R. M., Kamarck, M. E., Ramabhadran, T. V., Dreyer, R. N., Davis, G., Unterbeck, A., and Tamburini, P. P. (1991) *Biochemistry 30*, 10467−10478.
26. Hynes, T. R., Randal, M., Kennedy, L. A., Eigenbrot, C., and Kossiakoff, A. A. (1990) *Biochemistry 29*, 10018−10022.
27. Kitaguchi, N., Takahashi, Y., Oishi, K., Shiojiri, S., Tokushima, Y., Utsunomiya, T., and Ito, H. (1990) *Biochim. Biophys. Acta 1038*, 105−113.
28. Favre, I., Sun, Y., and Moczydlowski, E. (1999) *Methods Enzymol. 294*, 287−304.
29. Favre, I., and Moczydlowski, E. (1999) *J. Gen. Physiol. 113*, 295−320.

30. Vincent, J.-P., and Lazdunski, M. (1972) *Biochemistry 11*, 2967−2977.
31. Rühlmann, A., Kukla, D., Schwager, P., Bartels, K., and Huber, R. (1973) *J. Mol. Biol. 77*, 417−436.
32. Scheidig, A. J., Hynes, T. R., Pelletier, L., Wells, J. A., and Kossiakoff, A. A. (1997) *Protein Sci. 6*, 1806−1824.
33. Janin, J., and Chothia, C. (1976) *J. Mol. Biol. 100*, 197−211.
34. Beckmann, J., Mehlich, A., Schröder, W., Wenzel, H. R., and Tschesche, H. (1988) *Eur. J. Biochem. 176*, 675−682.
35. Stampe, P., Kolmakova-Partensky, L., and Miller, C. (1994) *Biochemistry 33*, 443−450.
36. Schreiber, G., and Fersht, A. R. (1995) *J. Mol. Biol. 248*, 478−486.
37. Guo, X., Uehara, A., Ravindran, A., Bryant, S. H., Hall, S., and Moczydlowski, E. (1987) *Biochemistry 26*, 7546−7556.
38. Toro, L., Ottolia, M., Stefani, E., and Latorre, R. (1994) *Biochemistry 33*, 7220−7228.
39. Murrell-Lagnado, R. D., and Aldrich, R. W. (1993) *J. Gen. Physiol. 102*, 949−975.
40. Schreiber, G., and Fersht, A. R. (1996) *Nat. Struct. Biol. 3*, 427−431.
41. Selkoe, D. J. (1990) *Science 248*, 1058−1060.
42. Castro, M. J. M., and Anderson, S. (1996) *Biochemistry 35*, 11435−11446.
43. Hubbard, S. J., Campbell, S. F., and Thornton, J. M. (1991) *J. Mol. Biol. 220*, 507−530.
44. Bode, W., and Huber, R. (1992) *Eur. J. Biochem. 204*, 433−451.
45. Sabharwal, A. K., Birktoft, J. J., Gorka, J., Wildgoose, P., Petersen, L. C., and Bajaj, S. P. (1995) *J. Biol. Chem. 270*, 15523−15530.
46. Bode, W., and Huber, R. (1975) *FEBS Lett. 56*, 139−143.
47. Lancelin, J.-M., Foray, M.-F., Poncin, M., Hollecker, M., and Marion, D. (1994) *Struct. Biol. 1*, 246−250.
48. Capasso, C., Rizzi, M., Menegatti, E., Ascenzi, P., and Bolognesi, M. (1997) *J. Mol. Recogn. 10*, 26−35.
49. Petersen, L. C., Birktoft, J. J., and Flodgaard, H. (1993) *Eur. J. Biochem. 214*, 271−279.
50. van de Locht, A., Bode, W., Huber, R., Le Bonniec, B. F., Stone, S. R., Esmon, C. T., and Stubbs, M. T. (1997) *EMBO J. 16*, 2977−2984.
51. Antonini, E., Ascenzi, P., Bolognesi, M., Gatti, G., Guarneri, M., and Menegatti, E. (1983) *J. Mol. Biol. 165*, 543−558.
52. Vincent, J.-P., and Lazdunski, M. (1976) *FEBS Lett. 63*, 240−244.
53. Borjigin, J., and Nathans, J. (1993) *Proc. Natl. Acad. Sci. U.S.A. 90*, 37−341.
54. Helland, R., Otlewski, J., Sundheim, O., Dadlez, M., and Smalas, A. O. (1999) *J. Mol. Biol. 287*, 923−942.
55. Bode, W., Schwager, P., and Huber, R. (1978) *J. Mol. Biol. 118*, 99−112.
56. Cox, D. H., Cui, J., and Aldrich, R. W. (1997) *J. Gen. Physiol. 110*, 257−281.
57. Diaz, L., Meera, P., Amigo, J., Stefani, E., Alvarez, O., Toro, L., and Latorre, R. (1998) *J. Biol. Chem. 273*, 32430−32436.
58. Cruz, L. J., Gray, W. R., Olivera, B. M., Zeikus, R. D., Kerr, L., Yoshikami, D., and Moczydlowski, E. (1985) *J. Biol. Chem. 260*, 9280−9288.
59. Becker, S., Prusak-Sochaczewski, E., Zamponi, G., Beck-Sickinger, A. G., Gordon, R. D., and French, R. J. (1992) *Biochemistry 31*, 8229−8238.
60. Chang, N. S., French, R. J., Lipkind, G. M., Fozzard, H. A., and Dudley, S. (1998) *Biochemistry 37*, 4407−4419.
61. Imredy, J. P., Chen, C., and MacKinnon, R. (1998) *Biochemistry 37*, 14867−14874.
62. Hoshi, T., Zagotta, W. N., and Aldrich, R. W. (1990) *Science 250*, 533−538.
63. Zagotta, W. N., Hoshi, T., and Aldrich, R. W. (1990) *Science 250*, 568−571.
64. Foster, C. D., Chung, S., Zagotta, W. N., Aldrich, R. W., and Levitan, I. (1992) *Neuron 9*, 229−236.
65. Knaus, H.-G., Folander, K., Garcia-Calvo, M., Garcia, M. L., Kaczorowski, G. J., Smith, M., and Swanson, R. (1994) *J. Biol. Chem. 269*, 17274−17378.
66. Wallner, M., Meera, P., and Toro, L. (1999) *Proc. Nat. Acad. Sci. U.S.A. 96*, 4137−4142.
67. Xia, X.-M., Ding, J. P., and Lingle, C. J. (1999) *J. Neurosci. 19*, 5255−5264.

BI992140V